Journal of
Materials Chemistry B

ROYAL SOCIETY
OF CHEMISTRY

PAPER

View Article Online
View Journal | View Issue

Check for updates

Cite this: *J. Mater. Chem. B*, 2024, **12**, 4427

# Injectable *in situ* gelling methylcellulose-based hydrogels for bone tissue regeneration†

Lorenzo Bonetti,[a] Silvia Borsacchi,*[bc] Alessandra Soriente,[d] Alberto Boccali,[a] Lucia Calucci,[bc] Maria Grazia Raucci[d] and Lina Altomare*[ae]

Injectable bone substitutes (IBSs) represent a compelling choice for bone tissue regeneration, as they can be exploited to optimally fill complex bone defects in a minimally invasive manner. In this context, *in situ* gelling methylcellulose (MC) hydrogels may be engineered to be free-flowing injectable solutions at room temperature and gels upon exposure to body temperature. Moreover, incorporating a suitable inorganic phase can further enhance the mechanical properties of MC hydrogels and promote mineralization, thus assisting early cell adhesion to the hydrogel and effectively guiding bone tissue regeneration. In this work, thermo-responsive IBSs were designed selecting MC as the organic matrix and calcium phosphate (CaP) or CaP modified with graphene oxide (CaPGO) as the inorganic component. The resulting biocomposites displayed a transition temperature around body temperature, preserved injectability even after loading with the inorganic components, and exhibited adequate retention on an *ex vivo* calf femoral bone defect model. The addition of CaP and CaPGO promoted the *in vitro* mineralization process already 14 days after immersion in simulated body fluid. Interestingly, combined X-ray diffraction and solid state nuclear magnetic resonance characterizations revealed that the formed biomimetic phase was constituted by crystalline hydroxyapatite and amorphous calcium phosphate. *In vitro* biological characterization revealed the beneficial impact of CaP and CaPGO, indicating their potential in promoting cell adhesion, proliferation and osteogenic differentiation. Remarkably, the addition of GO, which is very attractive for its bioactive properties, did not negatively affect the injectability of the hydrogel nor the mineralization process, but had a positive impact on cell growth and osteogenic differentiation on both pre-differentiated and undifferentiated cells. Overall, the proposed formulations represent potential candidates for use as IBSs for application in bone regeneration both under physiological and pathological conditions.

Received 15th October 2023,
Accepted 4th April 2024

DOI: 10.1039/d3tb02414h

rsc.li/materials-b

## 1. Introduction

Methylcellulose (MC) hydrogels are well-known biomaterials that have attracted significant attention in the fields of tissue engineering and regenerative medicine.[1] MC hydrogels exhibit lower critical solution temperature (LCST) behavior, undergoing a reversible thermo-responsive gelation process around their transition temperature ($T_t$ or $T_{gel}$). Upon heating, MC hydrogels show a transition from a sol (at $T < T_t$) to a gel state (at $T > T_t$), as a result of MC self-assembly into stiff fibrils that percolate into a fibrillar network. When the generated fibrils cool, they unbind and the MC gel returns to its original solution state.[2–6] MC hydrogels display peculiar features due to the weak nature of the interactions involved in the gelation process, including reversibility of the sol–gel transition and decreased cytotoxicity (due to the lack of chemical crosslinkers),[7] and low cost. Moreover, the possibility of easily tuning the $T_t$ of MC hydrogels makes them even more attractive. In this regard, it is known that pristine MC hydrogels display a $T_t$ in the 55–60 °C temperature range (*i.e.*, 2% w/v MC solution), far enough from physiological temperature to make them non-responsive to body temperature. However, $T_t$ can be simply modified by

---

[a] *Department of Chemistry, Materials, and Chemical Engineering "G. Natta", Politecnico di Milano, Piazza Leonardo da Vinci 32, 20133 Milano, Italy. E-mail: lina.altomare@polimi.it*

[b] *Institute of Chemistry of Organometallic Compounds (ICCOM), Italian National Research Council (CNR), Via G. Moruzzi 1, 56124 Pisa, Italy. E-mail: silvia.borsacchi@pi.iccom.cnr.it*

[c] *Center for Instrument Sharing of the University of Pisa (CISUP), Lungarno Pacinotti 43/44, 56126 Pisa, Italy*

[d] *Institute for Polymers, Composites and Biomaterials (IPCB), Italian National Research Council, Viale J.F. Kennedy 54, Mostra d'Oltremare Pad 20, 80125 Napoli, Italy*

[e] *National Interuniversity Consortium for Materials Science and Technology (INSTM), Via Giuseppe Giusti 9, 50121 Firenze, Italy*

† Electronic supplementary information (ESI) available. See DOI: **https://doi.org/10.1039/d3tb02414h**

acting on different parameters in the preparation of the hydrogels: the degree of substitution, MC concentration, and the presence of salts or additives (*e.g.*, other polymers, sugars) in solution are among the main players in this tuning.[1,2]

Injectable hydrogels have been largely investigated in several reviews,[8–10] displaying how different types of hydrogels may be prepared and how their properties (*e.g.*, gelling time, mechanical properties) can be modified according to the final application. In general, injectable hydrogels must be flowable and easily extrudable through needles or catheters, but this implies that they may be affected by poor mechanical properties. Moreover, only a few studies[11,12] address the issue of injectability, and the findings are controversial and challenging to compare, mainly due to variations in injection conditions (*e.g.*, injection rate, needle dimensions).

In this panorama, *in situ* gelling – or *in situ* forming – MC hydrogels may be engineered to be free-flowing injectable solutions at room temperature ($T < T_t$) and gels upon exposure to body temperature ($T \geq T_t$). Due to *in situ* gelation, MC hydrogels have specific benefits over standard injectable hydrogel formulations, including the potential to be minimally invasive, fill irregularly shaped voids, and ensure shape stability and excellent mechanical properties following injection.

In the field of bone tissue engineering, the addition of an inorganic phase (*e.g.*, calcium phosphates, CaPs, or bioglasses) can further improve the mechanical properties of MC hydrogels, also promoting mineralization, a property of paramount importance to assist early cell adhesion to the hydrogel and successfully guide bone tissue regeneration.[1,10]

In this scenario, MC hydrogels have been explored as injectable bone substitutes (IBSs) and two main approaches have been reported to produce MC-based IBSs: CaP loading and CaP nucleation and growth into MC-based hydrogels. In the first approach, CaPs were added directly into the MC hydrogel. Following this approach, Oğuz *et al.*[13] proposed IBSs prepared from MC (8% (w/v)), gelatin (2.5% (w/v)), and sodium citrate (3% (w/v)) loaded with different amounts of CaPs (0–50 wt%), obtaining injectable formulations with improved mechanical performance (five-fold increase in compressive strength compared to pristine MC hydrogels) and capable of forming a gel around 37 °C. Interestingly, the limit for injectability was achieved for 50% CaP loading. The same hydrogel formulation, with the addition of graphene oxide (GO), was also investigated for the bioactive potential of GO.[14] In the second approach, precursor salts (*i.e.*, $CaCl_2$ and $Na_2HPO_4$), added to the MC solutions, supported both the *in situ* nucleation of CaPs and the tuning of the $T_t$ of the resulting MC hydrogels. Following this approach, Kim and co-workers[11,15,16] obtained CaP-loaded MC hydrogels *via* an *in situ*, one-pot synthesis process. The obtained hydrogels displayed $T_t$ lower than body temperature (28–29 °C) and *in vitro* biocompatibility. The *in vivo* study in a rabbit calvarial defect model indicated a superior regeneration rate of new mature bone in the MC-CaP composite hydrogel compared with the pristine MC hydrogel. Interestingly, injectability tests revealed a maximum injection force lower than 30 N at room temperature, representing the upper limit for manual injection of an IBS.[11] Overall, these studies reveal that MC-based hydrogels are promising materials for filling bone tissue deficiencies and assisting bone tissue regeneration.

The aim of the present work was to develop novel IBSs selecting: (i) MC as the organic matrix, to provide injectable and *in situ* gelling hydrogels; (ii) calcium phosphate (CaP) or CaP modified with graphene oxide (CaPGO) as the inorganic component, to mimic the native environment of bone tissue and offer additional biological properties in the case of CaPGO. These biocomposites were designed to preserve the gels injectability even after loading with the inorganic phases, as well as to promote the formation of bone substitute phases upon mineralization. The prepared hydrogels were first characterized from a rheological point of view to assess their thermoresponsive behavior and their viscoelastic properties prior to and after gelation. Then, injectability tests were carried out to measure the force needed to extrude them through an 18 G needle and their retention capacity was evaluated on an *ex vivo* calf femoral bone defect model. Moreover, the *in vitro* mineralization of the hydrogels was investigated by performing X-Ray Diffraction (XRD) and Solid State NMR (SSNMR) experiments on samples taken at selected mineralization times. XRD allowed crystalline phases to be identified, while by exploiting SSNMR it was possible to detect and quantify crystalline, nanocrystalline, and amorphous phases. The possibility of easily observing $^{31}P$ and $^{1}H$ nuclei, whose NMR properties (*e.g.*, chemical shift, dipolar interactions, relaxation times) are directly related to the structural and dynamic features of their local environment, makes SSNMR a very powerful investigation technique for bone-related materials, unique in the panorama of MC-based injectable IBSs. In this work, by combining XRD and SSNMR, the phosphate-containing phases formed during the *in vitro* mineralization process of CaP- and CaPGO-loaded MC gels have been identified and quantified, characterizing their time evolution and the effect of the presence of GO. Lastly, an *in vitro* biological characterization was carried out, investigating the impact of MC-based formulations on cell proliferation and osteogenic differentiation.

## 2. Experimental section

### 2.1. Materials

Unless stated, all reagents were purchased from Merck (Merck Life Science S.r.l., Italy) and used without further purification.

### 2.2. Hydrogel preparation

MC hydrogels were prepared according to previously reported procedures.[17–19] Briefly, MC (2% w/v) was added to a hot (55 °C) $Na_2SO_4$ water solution (150 mM) under stirring. This formulation was selected on the basis of both our previous studies on MC hydrogels[1,17,20–22] and a composition optimization investigation centred on the swelling behavior and gelation temperature of MC hydrogels prepared with a $Na_2SO_4$ concentration ranging from 100 to 200 mM (S1, ESI†). The obtained solution was cooled to room temperature under stirring, then stored in the refrigerator (4 °C) overnight to allow complete MC hydration. To prepare the biocomposites, CaP and CaPGO powders were produced using sol–gel technology as previously reported,[12,23] starting from calcium nitrate tetrahydrate [$Ca(NO_3)_2 \cdot 4H_2O$] and diammonium hydrogen phosphate [$(NH_4)_2HPO_4$], as precursors for $Ca^{2+}$ and $PO_4^{3-}$, respectively, with a Ca/P molar ratio in the range of 1.6–1.7. By including GO (1.5 wt%, Nanesa s.r.l.) during the *in situ* sol–gel synthesis of CaP, CaPGO was obtained. The addition of CaP and CaPGO powders (1% (w/v)) to the gel was carried out with two syringes, one loaded with the MC hydrogel and the other with the powder suspension in deionised (DI) water. This set-up was studied to allow working and mixing under sterile conditions. The two syringes were connected with a three-way Luer Stopcock and mixing was achieved through 50 passes between the syringes, until a uniform gel was obtained.[12] From this point on, the samples analysed will be referred to as MC, MC-CaP, and MC-CaPGO.

### 2.3. Rheological tests

A thorough rheological characterization was performed using a rotational rheometer (MCR 302, Anton Paar GmbH, Graz, Austria) equipped with a parallel plate geometry ($\varnothing$: 25 mm, gap = 1 mm).

Amplitude sweep tests were carried out on each formulation to identify the linear viscoelastic region (LVR) by applying an oscillatory strain ($\gamma$) in the 0.01–10% range, setting a frequency ($\nu$) of 1 Hz, at 20 and 40 °C.

Then, to identify the transition temperature ($T_{gel}$) of the composite MC gels, temperature sweep tests were carried out in the 20–50 °C range, with a heating ramp of 2 °C $min^{-1}$, $\gamma$ = 1%, $\nu$ = 1 Hz. The transition temperatures were identified from the storage ($G'$) and loss moduli ($G''$) as the crossover point ($G' = G''$).[24]

Time sweep tests were carried out to identify the gelation time ($t_{gel}$) of the gels. Before starting the test, the temperature was set at 20 °C; then, the temperature was impulsively increased to 37 °C and the viscoelastic properties of the materials were measured in a time window of 300 s, $\gamma$ = 1%, $\nu$ = 1 Hz. The $t_{gel}$ was identified from the crossover point ($G' = G''$).

Lastly, the viscosity of the samples was measured *via* shear rate sweep tests, by applying a shear rate ($\dot{\gamma}$) ramp in the 0.1–1000 $s^{-1}$ range at 20 °C.

### 2.4. Injectability tests

Injectability tests were carried out on a uniaxial tensile testing machine (MTS 1/MH, 5 kN load cell, MTS System, Eden Prairie, MN, USA) in compression configuration. The hydrogels were loaded into 5 mL syringes fitted with 18 G needles and positioned in a previously reported custom experimental set-up.[12] The measurements were carried out at room temperature (20 °C). A pre-load of 0.15 N was set, then the syringe piston was compressed at a rate of 0.6 mm $s^{-1}$ and the force applied on it was recorded. The resulting force value was then multiplied by a factor of 1.1 to take into account the resistance of biological tissues toward injection.[11]

### 2.5. *Ex vivo* tilt tests

Calf femurs were purchased from a local butcher. Bone slices (15 mm in thickness) were obtained from calf femoral heads using a die grinder (Dremel® 3000) equipped with a 32 mm cut-off wheel. A hemispherical hole, 6 mm in diameter, was then drilled into the cancellous bone of each slice using the die grinder equipped with a 3.2 mm tungsten carbide cutter ball tip. Subsequently, each cavity was filled with 500 μL of MC, MC-CaP, or MC-CaPGO. The samples were then incubated at either 20 or 37 °C for 3 h, followed by tilt tests.[20] In the test, the samples were inverted (180° rotation) and any flow of the MC formulations from the bone cavity was noted.

### 2.6. *In vitro* mineralization tests

Mineralization tests were performed by immersing the hydrogels in simulated body fluid (SBF), prepared according to the protocol described by Kokubo *et al.*[25] For the evaluation of mineralization, aliquots (0.5 mL) of composite hydrogels were added in dialysis tubes (10 mm width, $M_w$ cut-off = 14 kDa), submerged in 10 mL of SBF inside 15 mL Falcon tubes, and kept under stirring (37 °C, 50 rpm) in a shaking incubator (SKI 4, Argo Lab, Giorgio Bormac S.r.l. Carpi MO, Italy). The SBF was renewed every 48 h and, at selected time points (7, 14, 28 days), the specimens were withdrawn and washed 3 times (24 hours total washing time) with DI water inside the dialysis tubes to remove soluble inorganic species.

For the XRD and SSNMR experiments, the washed specimens were first frozen at −20 °C, then freeze-dried (−40 °C, <0.5 mbar). Hereafter, these samples will be indicated as MC_*x*d, MC-CaP_*x*d, and MC-CaPGO_*x*d, where *x* is the mineralization time (in days) and 0 days refers to samples that were not immersed in SBF.

**2.6.1. X-ray diffraction measurements.** X-ray Diffraction (XRD) analysis was performed using a diffractometer (Empyrean, Malvern Panalytical Ltd, Malvern, UK) equipped with Bragg Brentano geometry (Cu-Kα1 radiation, $\lambda$ = 0.154056 nm). The X-ray diffraction patterns were collected in the 0–80° $2\theta$ range (0.02° step size, 20 s per step scan speed, room temperature). Each measurement was performed in triplicate in order to increase the signal-to-noise ratio.

**2.6.2. Solid state NMR measurements.** SSNMR spectra were recorded on a Bruker Avance Neo spectrometer working at Larmor frequencies of 500.13 and 202.46 MHz for $^{1}H$ and $^{31}P$, respectively, using a double-resonance Magic Angle Spinning (MAS) probe head accommodating rotors with an external diameter of 4 mm. $^{31}P$ Direct Excitation (DE) MAS spectra were recorded under high-power decoupling from $^{1}H$ nuclei, using a recycle delay of 1200 s and accumulating 4 transients. $^{31}P$ Cross Polarization (CP) MAS spectra were recorded using contact time values of 0.5 and 2 ms, a recycle delay of 6 s and accumulating 80 transients. $^{1}H$ MAS spectra were recorded with a DE pulse sequence, and a recycle delay of 6 s and 4 transients. Unless otherwise stated, all spectra were recorded at a MAS frequency of 10 kHz, using air as spinning gas, at room temperature. The chemical shift scale was referenced to the signal of adamantane at 38.48 ppm for $^{13}C$ and calculated from the same value for all other nuclei, using the unified scale recommended by IUPAC.[26] Spectral deconvolution was performed using MNova software.

### 2.7. *In vitro* biological characterization

MC hydrogels were prepared using a filter sterilized $Na_2SO_4$ solution (0.22 μm pore size filter) and UV light sterilized MC, CaP, and CaPGO powders (2 h).

**2.7.1. *In vitro* cell culture and biocompatibility.** Biological investigations were performed using murine osteoblast cells (7F2) and human mesenchymal stem cells (hMSC). In 75 $cm^2$ cell culture flasks, cells were cultured in high glucose Dulbecco's Modified Eagle's Medium (DMEM) supplemented with 10% Fetal Bovine Serum (FBS), antibiotic solution (100 g $mL^{-1}$ streptomycin, 100 U $mL^{-1}$ penicillin), and 2 mM L-glutamine. The culturing conditions were maintained at 37 °C with 5% $CO_2$ and 95% humidity to achieve confluence.

To create a suitable microenvironment for cell growth within the formulations (MC, MC-CaP, and MC-CaPGO), DMEM powder was added. Subsequently, cells (7F2: $5 \times 10^4$; hMSC: $2 \times 10^4$) were resuspended in 20 μL of FBS and inoculated into 200 μL of each formulation at room temperature in non-adherent 24-well plates. The plates were then incubated (37 °C, 5% $CO_2$, 95% humidity) to induce the sol–gel transition. Following this, 2 mL of medium was added to each well and incubated for different time intervals.

The *in vitro* biocompatibility of the MC-based formulations was evaluated using the Alamar Blue assay (Life Technologies, Italy) at 3, 7, and 14 days, according to the manufacturer's protocol. Fluorescence ($\lambda_{ex}$ = 560 nm; $\lambda_{em}$ = 590 nm) was measured using a spectrophotometer (Victor X3, PerkinElmer, Italy).

**2.7.2. *In vitro* cell differentiation: alkaline phosphatase and osteocalcin.** The *in vitro* osteogenic activity of the hydrogel formulations (MC, MC-CaP, and MC-CaPGO) was evaluated by assessing both early (alkaline phosphatase) and late (osteocalcin) markers of osteogenesis in basal medium without the presence of external growth factors.

First, alkaline phosphatase (ALP) activity within the gels was examined at 3, 7, and 14 days of culture. To quantify the ALP levels, cells were lysed using a cell lysis buffer, and the ALP activity was measured using the SensoLyte® pNPP Alkaline Phosphatase Assay kit (AnaSpec, DBA, Italy) following the manufacturer's instructions. Absorbance readings were taken in a 96-well plate at 405 nm using a spectrophotometer (Victor X3, PerkinElmer, Italy). The nanomolar (nM) ALP concentration was then calculated based on a standard curve. Next, to normalize the ALP values, the amount of double-stranded DNA (dsDNA) was quantified using a PicoGreen™ dsDNA quantification kit (Life Technologies, Italy). Fluorescence readings were recorded at 502/523 nm using a spectrophotometer (Victor X3, PerkinElmer, Italy). A calibration curve of a λ-dsDNA standard in a buffer of 10 mM Tris, 1 mM EDTA, pH = 7.5 was used to quantify dsDNA. The results of the ALP activity were reported as the nanomolar concentration of ALP normalized to the micrograms of total DNA content (nM ALP/μg DNA).

Additionally, osteocalcin levels, produced by hMSCs within the gels at 7 and 14 days, were analyzed using an ELISA kit (Elabscience, Italy) following the manufacturer's protocol. The optical density (OD value) was determined at 450 nm (Victor X3, PerkinElmer, Italy). The results are expressed as nanograms of osteocalcin on micrograms of total DNA content (ng OCN/μg DNA).

### 2.8. Statistical data analysis

Where possible, tests were run in triplicate ($n$ = 3). Data are expressed as mean ($M$) ± standard deviation (SD). To compare the data, $t$-tests or one-way ANOVA with Tukey's *post hoc* tests were used, considering a significance level of $\alpha = 0.05$.

## 3. Results and discussion

### 3.1. Rheological, injectability, and retention properties of MC hydrogels

In order to test the applicability of the MC hydrogels loaded with CaP or CaPGO as injectable bone substitutes, it is fundamental to characterize their rheological and injectability properties. Toward this aim, storage and loss moduli were measured on MC, MC-CaP, and MC-CaPGO in amplitude, temperature, and time sweep tests, determining the viscoelastic behavior at room and physiological temperature, as well as the gelation temperature and time. Moreover, the viscosity of the samples was measured *via* shear rate sweep tests and compared with the outcomes of the injectability tests, carried out under the operational conditions used in surgery.

Shear strain tests were conducted to determine the Linear Viscoelastic Region (LVR) of MC, MC-CaP, and MC-CaPGO samples (S2, ESI†).[20,21] As an outcome, a strain value $\gamma = 1\%$ was selected for all the subsequent tests.

To quantitatively evaluate $T_{gel}$ of the three formulations, temperature sweep tests were carried out between 20 and 50 °C, applying a heating ramp of 2 °C $min^{-1}$ (Fig. 1A1–A3). The $T_{gel}$ was determined from the crossover point between the conservative and the loss modulus (*i.e.*, $G' = G''$), where a transition from the sol phase ($G' < G''$) to the gel phase ($G' > G''$) occurs. A similar trend is detected in all the temperature sweep curves: for $T < T_{gel}$, a slight decrease of the viscoelastic parameters occurs, due to partial disentanglement of the MC chains upon shear stress; for $T > T_{gel}$, an increase of $G'$ occurs due to the aggregation of MC into stiff fibrils and percolation into a fibrillar network (*i.e.*, sol–gel transition).[11,15,17,18] The addition of CaP and CaPGO seems not to impact on the $T_{gel}$, which is 34–35 °C for the composites and 36 °C for MC (Table 1).

Then, a time sweep test was performed to quantitatively assess the gelation time, $t_{gel}$, of the three formulations (Fig. 1B1–B3). To replicate the injection process in the human body, the temperature was first set at 20 °C (operation room temperature) and then rapidly raised to 37 °C. In this regard, the standard ISO 5833/1-1999-E identifies an *in situ* gelling filler as clinically suitable when its $t_{gel}$ is lower than 15 min.[27] All three tested formulations displayed a gelation time of about 90

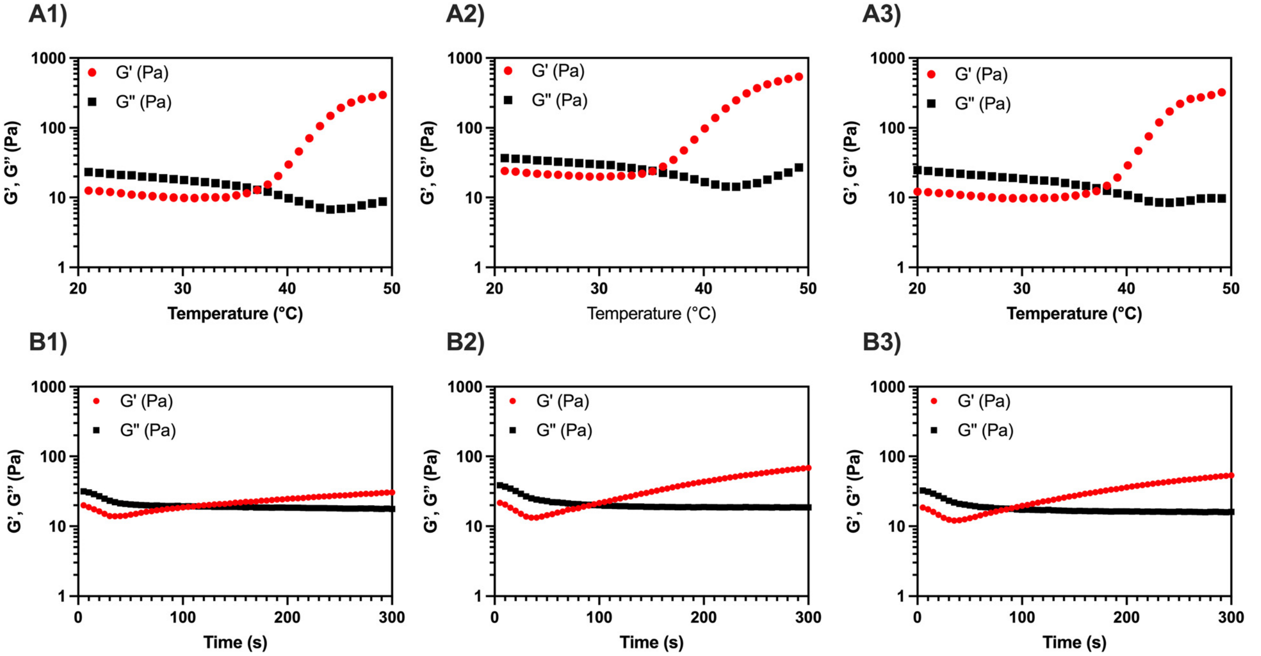

Fig. 1 Representative temperature sweep tests on (A1) MC, (A2) MC-CaP, and (A3) MC-CaPGO formulations. The tests were carried out in the 20–50 °C range (2 °C min$^{-1}$ ramp), $\gamma$ = 1%, $\nu$ = 1 Hz. Representative time sweep tests on (B1) MC, (B2) MC-CaP, and (B3) MC-CaPGO formulations. The tests were carried out in a time window of 300 s, $\gamma$ = 1%, $\nu$ = 1 Hz.

Table 1 Gelation temperature ($T_{gel}$) and gelation time ($t_{gel}$) for MC, MC-CaP, and MC-CaPGO formulations

| | MC | MC-CaP | MC-CaPGO |
|---|---|---|---|
| $T_{gel}$ (°C) | 35.8 ± 2.3 | 34.6 ± 0.7 | 34.5 ± 3.7 |
| $t_{gel}$ (s) | 98.8 ± 20.2 | 86.7 ± 2.9 | 85.0 ± 5.0 |

s, without significant differences induced by the addition of the inorganic powders (Table 1). On the other hand, a reduction in the setting time for MC hydrogels containing GO has been reported by Oğuz *et al.*,[28] but this variation can be ascribed both to the presence of free GO in the hydrogel formulation and to the higher amount of GO in the gel (used to enhance both biological response and rheological characteristics) compared to the present work.

During *in situ* gelling, thermo-responsive systems are generally formulated to be free-flowing (*i.e.*, injectable) at room temperature ($T < T_{gel}$), and readily gel upon exposure to body temperature ($T \geq T_{gel}$).[1] All the MC-based formulations here reported, displaying a $T_{gel}$ < 37 °C and a $t_{gel} \ll 15$ min, lend themselves well as injectable fillers.

Moreover, the viscosity of MC, MC-CaP, and MC-CaPGO was analyzed in rotational mode, applying a shear rate in the 0.1–1000 s$^{-1}$ range (Fig. 2). All the samples exhibit shear-thinning behavior in this range, characterized by a significant decrease in viscosity as the shear rate increases. This behavior, characteristic of non-Newtonian fluids, indicates the disruption of the MC hydrogel network,[12] and is of pivotal importance in the design of injectable hydrogels.[1,29]

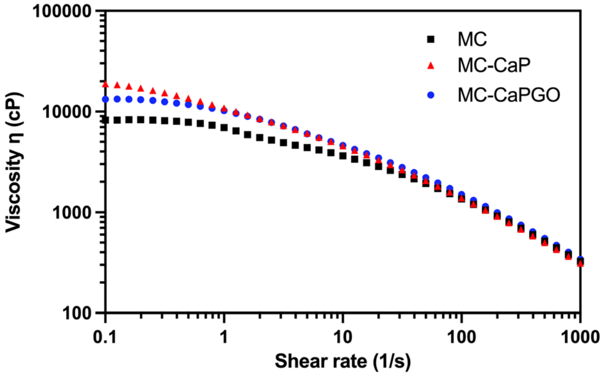

Fig. 2 Representative flow curves for MC, MC-CaP, and MC-CaPGO formulations. The tests were carried out at 20 °C, applying a shear rate ramp from 0.1 to 1000 s$^{-1}$.

Following the rheological characterization, injectability tests were carried out on MC, MC-CaP, and MC-CaPGO hydrogels by loading them into 5 mL sterile syringes equipped with an 18 G needle. The tests were carried out at 20 °C, setting the crosshead speed of the MTS apparatus at 0.6 mm s$^{-1}$ to mimic the operational conditions during surgery.[12,30,31] The obtained curves (Fig. 3), expressed as force *vs.* extension, display the same trend for all samples: after an initial exponential increase of the force value, associated to the extrusion of the hydrogel throughout the needle, a force plateau ($F_{mean}$) is reached. No significant differences were detected among the three formulations, which display $F_{mean}$ values of about 11 N (Table 2), in accordance with similar hydrogel

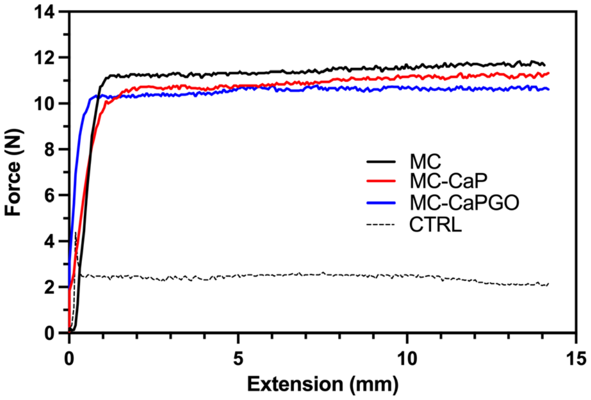

Fig. 3 Representative injectability tests for MC, MC-CaP, and MC-CaPGO formulations. CTRL = empty syringe. The hydrogel formulations were extruded through an 18 G needle at 20 °C at a crosshead speed of 0.6 mm $s^{-1}$, measuring the force needed for the process.

Table 2 Force values obtained from injectability tests for MC, MC-CaP, and MC-CaPGO formulations. Data are expressed as $F_{mean}$, indicating the force achieved at plateau. The values reported in this table are corrected by a factor 1.1 to consider the resistance of biological tissues to injection[11]

| | MC | MC-CaP | MC-CaPGO | CTRL |
|---|---|---|---|---|
| $F_{mean}$ (N) | 11.7 ± 0.2 | 11.0 ± 0.1 | 10.6 ± 0.1 | 2.2 ± 0.4 |

formulations.[11,12] Interestingly, the $F_{mean}$ values settle far below 30 N, commonly recognized as the upper force limit for manual injection of injectable materials.[15,32,33] Moreover, the loading of CaP and CaPGO powders into MC hydrogel did not lead to any obstruction of the needle, thus indicating that the proposed formulations can be effortlessly injected *in vivo* at a reasonable rate.

The retention capacity of the developed hydrogel formulations (MC, MC-CaP, MC-CaPGO) was evaluated on an *ex vivo* calf femoral bone defect model. Bone defects were filled with the hydrogel formulations and incubated (20 or 37 °C, 3 h). Bone samples were then tilted to observe the flow of the MC formulations from the bone cavity (Fig. 4 and Videos S1–S6, ESI†). All the formulations incubated at 20 °C rapidly flowed after inversion (Fig. 4A1–A3), as a consequence of the low viscosity in the sol state.[20] Conversely, the increase of temperature (37 °C) prevented any flow of the MC formulations from the bone defects (Fig. 4B1–B3), suggesting optimal retention in the defect site induced by the sol–gel transition.[20]

Considering the results of the rheological, injectability and retention tests, it is evident that all the developed formulations have several benefits over conventional hydrogels and scaffolds, including the ability to fill irregularly shaped cavities (such as bone deformities) and guarantee continuity (mechanical and physicochemical features) in the host tissue, and may be implanted using minimally invasive procedures. The addition of CaP and CaPGO maintains the gelation and injectability properties of the hydrogels at values suitable for IBSs. Moreover, CaP and CaPGO can promote the *in vivo* mineralization processes, leading to the deposition of a new bone matrix in the defect area.[1,11,13,15,16,34]

### 3.2. *In vitro* mineralization

To evaluate the effectiveness of CaP and CaPGO in enhancing the hydrogels' bioactivity in bone tissue regeneration, MC, MC-CaP and MC-CaPGO were subjected to a mineralization process in SBF up to 28 days, mimicking the mineralization process that occurs in native bone tissue.

The phosphate-containing phases formed in the mineralization process were identified and characterized in detail by means of XRD and SSNMR experiments, carried out on samples taken at selected mineralization times, washed, and freeze-dried (samples indicated as MC_*x*d, MC-CaP_*x*d, and MC-CaPGO_*x*d, where *x* is the mineralization time in days). While

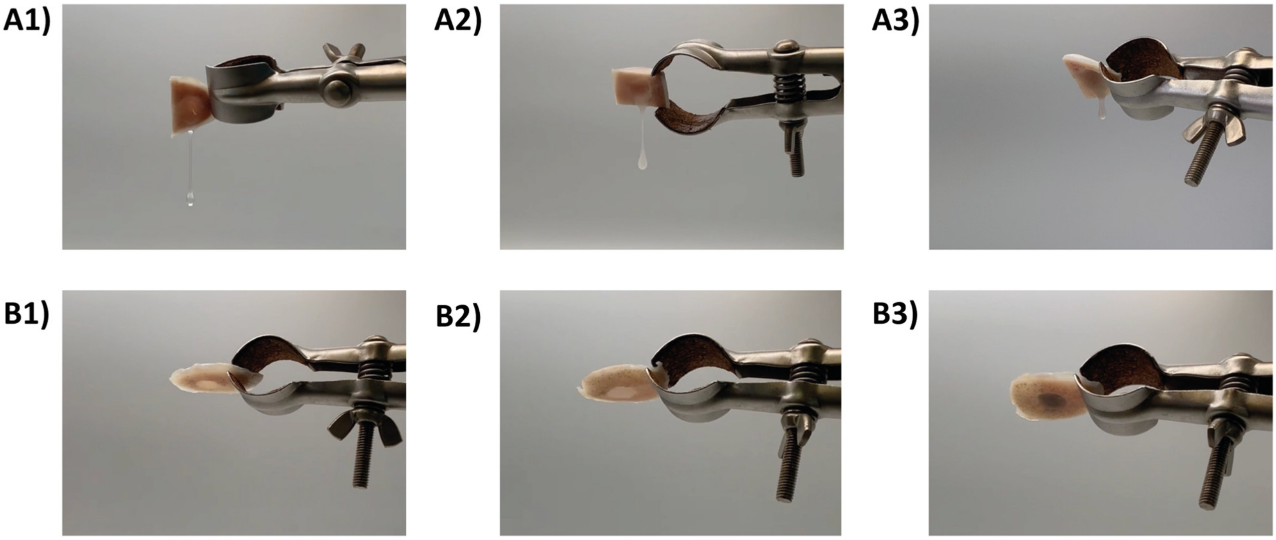

Fig. 4 *Ex vivo* tilt tests, displaying the flowability of the formulations as a function of temperature. Tests carried out at 20 °C on (A1) MC, (A2) MC-CaP, and (A3) MC-CaPGO; tests carried out at 37 °C on (B1) MC, (B2) MC-CaP, and (B3) MC-CaPGO.

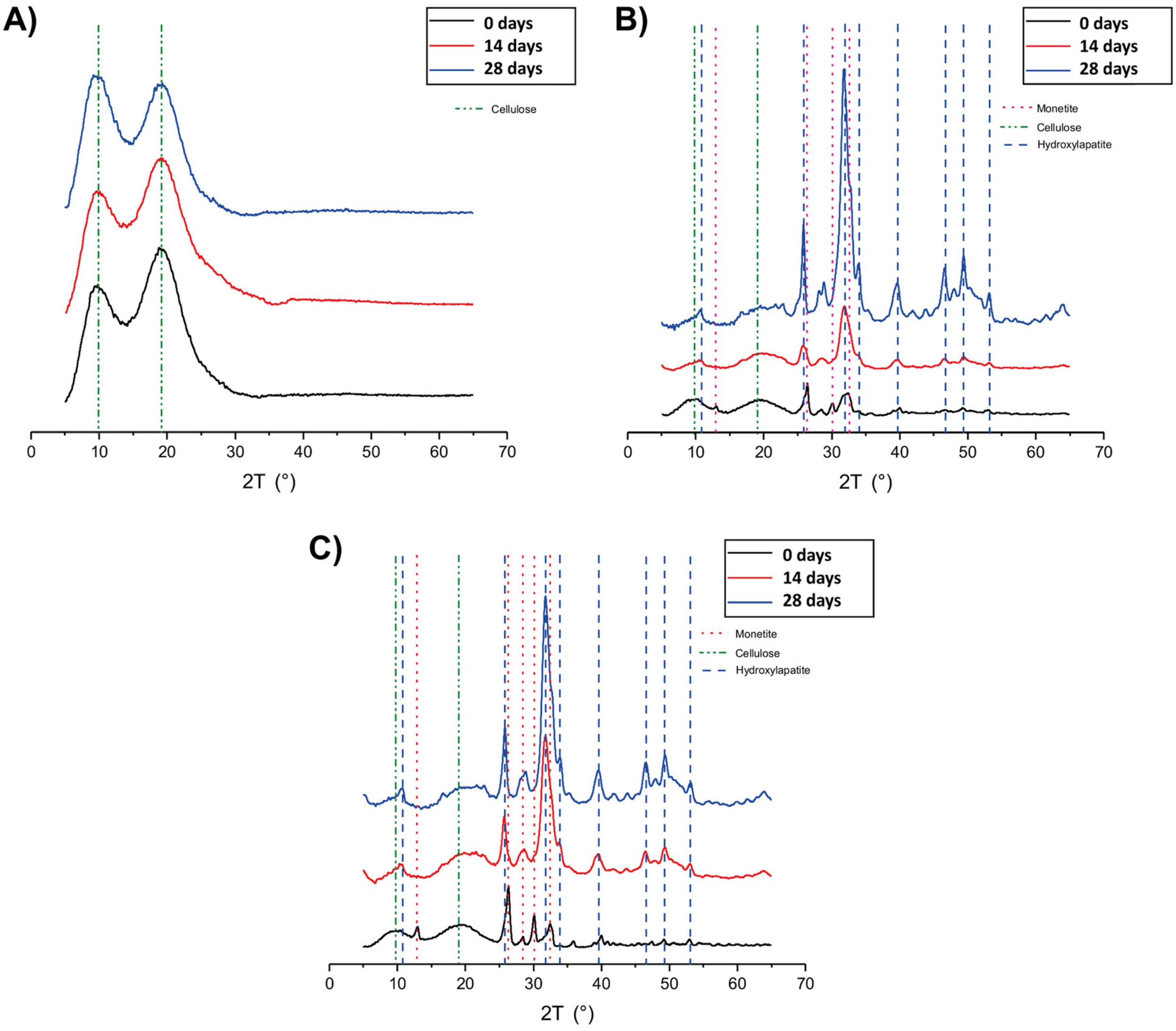

Fig. 5 XRD patterns of (A) MC_*x*d, (B) MC-CaP_*x*d, and (C) MC-CaPGO_*x*d formulations at selected time points.

the XRD analysis allows crystalline phases to be detected, SSNMR can also reveal the presence of amorphous phases and provide a quantitative determination of all the phases.

The XRD analysis of MC_*x*d samples (Fig. 5A) revealed that the peaks corresponding to MC (green dotted lines) remain consistent up to 28 days in SBF. No evidence of hydroxyapatite ($Ca_{10}(PO_4)_6(OH)_2$) formation was observed, indicating that MC itself does not undergo mineralization. In the diffractograms of MC-CaP_*x*d (Fig. 5B) and MC-CaPGO_*x*d (Fig. 5C), beside the MC peaks, signals of monetite ($CaHPO_4$) are observed (red dotted lines) at the initial stages of mineralization, owing to the presence of monetite in CaP and CaPGO (*vide infra*). The characteristic diffraction pattern of hydroxyapatite[12,35] at $2\theta$ angles of 10.6°, 25.9°, 31.8°, 32.8°, 34.0°, 39.6°, 46.7°, 49.5°, and 53.2° (blue dotted lines) becomes detectable already after 7 days of SBF immersion (data not shown). For longer immersion times (up to 28 days), the hydroxyapatite peak intensity progressively increases, while the peaks related to the monetite phase almost disappear. This indicates that the presence of CaP induces the formation of hydroxyapatite, replicating the mineralization process observed in native bone tissue.[35]

The XRD patterns of MC-CaPGO_*x*d samples resemble those of MC-CaP_*x*d, suggesting that the presence of GO does not influence the mineralization process. Similar observations have been reported by Oğuz *et al.*,[13] who showed that the addition of GO to a MC hydrogel did not cause changes to the XRD pattern.

A more complete picture of the phosphate-containing phases formed during the mineralization of the hydrogels was obtained from $^{31}P$ and $^{1}H$ SSNMR experiments. Indeed, SSNMR played a significant role in the progress of knowledge of the complex chemical structure of bone and bone-related materials, as well as in understanding the mineralization processes of biomaterials.[36–44]

The $^{31}P$ MAS spectra of MC_*x*d samples do not show any signals, confirming that mineralization does not occur in pristine MC hydrogels. In Fig. 6 the quantitative $^{31}P$ DE-MAS

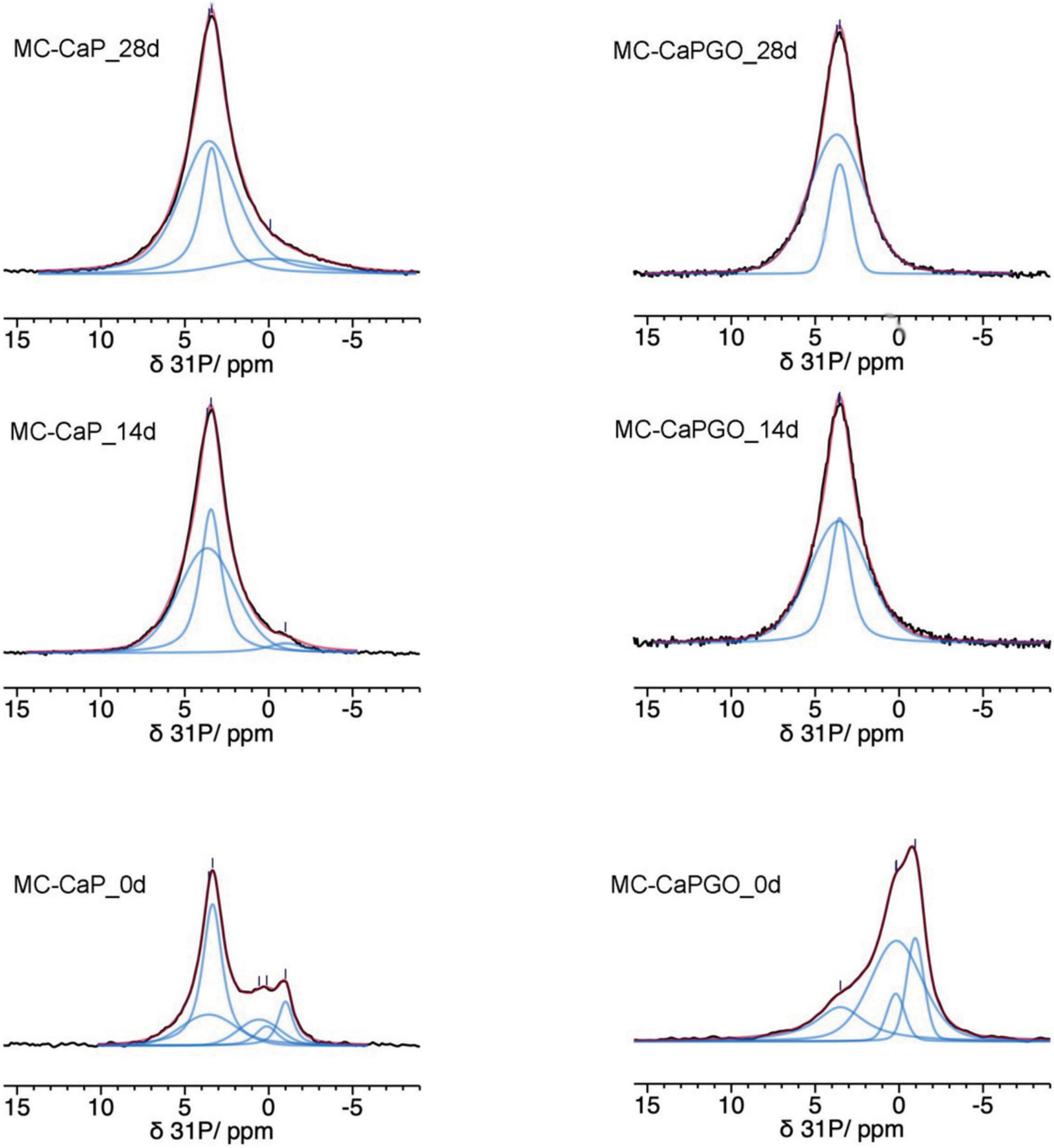

Fig. 6 $^{31}$P quantitative DE-MAS NMR spectra (black) of the indicated samples. The calculated spectra are shown as red traces, while the single peaks are in blue.

spectra of MC-CaP_*x*d samples, with $x$ = 0, 14, 28, are shown. The spectrum of the non-mineralized sample, MC-CaP_0d, shows peaks at about −1 and 0.5 ppm, ascribable to monetite arising from the CaP powder (S3, ESI†), and one intense peak at 3.3 ppm, due to hydroxyapatite.[41,45–48] A spectral deconvolution performed through a fitting procedure allowed us to recognize that the signal at 3.3 ppm results from the superimposition of two peaks (both with the same chemical shift): the first one with a linewidth of 270 Hz and a Lorentzian lineshape, already observed in the spectrum of CaP (Fig. S4, ESI†) and ascribable to crystalline hydroxyapatite; the second one with a linewidth of 820 Hz and a Gaussian lineshape, ascribable to an amorphous calcium phosphate phase (ACP), already observed to form on the pore walls of $CaO–SiO_2–P_2O_5$ mesoporous bioactive glasses soaked in SBF.[48–50] It is worth mentioning that the observed composite signal could also be ascribed to nanocrystalline hydroxyapatite, which is reported to be constituted by a core of crystalline hydroxyapatite and a surface layer of ACP.[37] The

Table 3 Total phosphorus amount (a.u.) and distribution in the different phases present in the indicated samples, obtained from the analysis of the quantitative $^{31}$P DE-MAS spectra reported in Fig. 6. For the sake of simplicity, the total amount of P in MC-CaP_0d was set to 1. The uncertainty on the results is within ±5%

| Sample | Total P | P of monetite | P of hydroxyapatite | P of ACP |
|---|---|---|---|---|
| MC-CaP_0d | 1 | 0.27 | 0.43 | 0.30 |
| MC-CaP_14d | 2 | 0.10 | 0.76 | 1.14 |
| MC-CaP_28d | 2.5 | 0 | 0.73 | 1.80 |
| MC-CaPGO_0d | 1.3 | 1 | 0 | 0.30 |
| MC-CaPGO_14d | 1.9 | 0 | 0.59 | 1.31 |
| MC-CaPGO_28d | 2.4 | 0 | 0.50 | 1.90 |

formation of ACP, not observed in CaP (S3, ESI†), is clearly favored by the environment created by the hydrogel and it is of particular interest for its biomimetic tissue-bonding ability. Moreover, the comparison of the $^{31}$P DE-MAS spectrum of MC-CaP_0d with that of CaP (Fig. S4, ESI†) also shows that the hydrogel strongly favors the formation of hydroxyapatite instead of monetite.

A comparison of the normalized total spectral areas of MC-CaP_0d, MC-CaP_14d and MC-CaP_28d (Table 3) shows that soaking the MC-CaP hydrogel in SBF results in a progressive increase of the total amount of phosphate-containing phases, indicating that mineralization proceeds. In fact, the number of detected $^{31}$P nuclei doubles in the first 14 days and then further slightly increases up to 28 days. From the relative intensities of the peaks present in the spectra of the three samples, it is possible to infer that, after 14 days in SBF, the content of monetite is substantially reduced and ACP and hydroxyapatite are the main phases present. From 14 to 28 days, hydroxyapatite does not increase, while ACP still grows. The relative percentages of ACP and crystalline hydroxyapatite, in terms of P atoms, obtained from the areas of the respective signals, change from 41/59 in MC-CaP_0d to 60/40 in MC-CaP_14d and 71/29 in MC-CaP_28d, indicating that the mineralization preferentially results in the formation of ACP.

Useful information is also provided by $^{1}$H MAS spectra (Fig. 7). For all MC-CaP_*x*d samples, a narrow peak is observed at about 0.6 ppm, which can be ascribed to –OH hydrogens of hydroxyapatite,[45,48] observed also in CaP (Fig. S5, ESI†). The most intense signal is centered at a chemical shift of 4.3 ppm, and it displays a narrow and a broad component. This signal is also present in the spectrum of MC_0d; thus, it must be partly ascribed to hydrogens of MC. However, the intensity of the broad component of this signal visibly increases moving from MC_0d to MC-CaP_0d and also increases with mineralization time, suggesting that hydrogens of ACP also contribute to this signal.

In this context it is interesting to compare the $^{31}$P DE-MAS spectrum of MC-CaP_28d with CP-MAS ones, in which signals of P atoms in spatial proximity to hydrogens are enhanced (Fig. 8). In agreement with the literature,[48] the CP-MAS spectrum recorded with a short contact time of 0.5 ms, which favors the signals of $^{31}$P nuclei within a few Å from $^{1}$H nuclei, highlights the broad signal of ACP, indicating that this phase contains many more hydrogens than hydroxyapatite. However, by recording the CP-MAS spectrum with a longer contact time (2 ms), the $^{1}$H to $^{31}$P magnetization transfer is allowed to proceed also for $^{31}$P nuclei at larger distances from $^{1}$H ones.

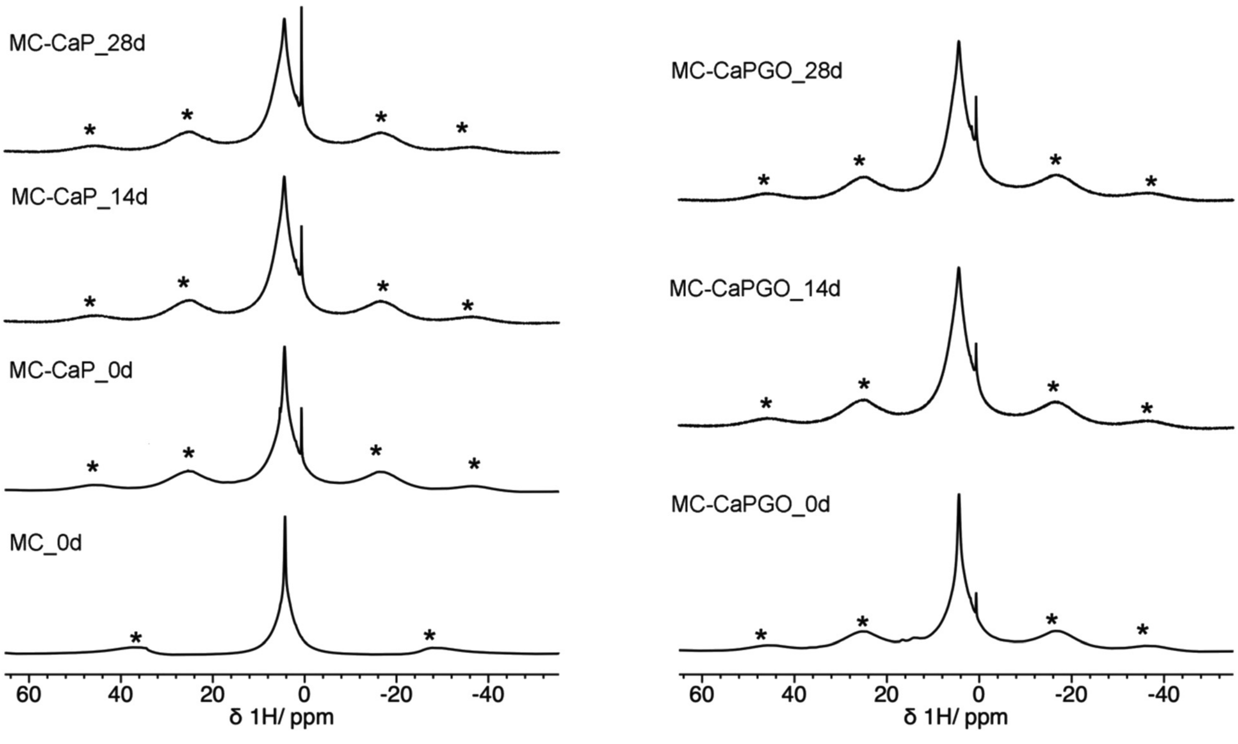

Fig. 7 $^{1}$H MAS spectra of MC_0d (MAS frequency of 15 kHz) and of MC-CaP_*x*d and MC-CaPGO_*x*d samples. Asterisks indicate spinning sidebands of the broad peak at 4.3 ppm.

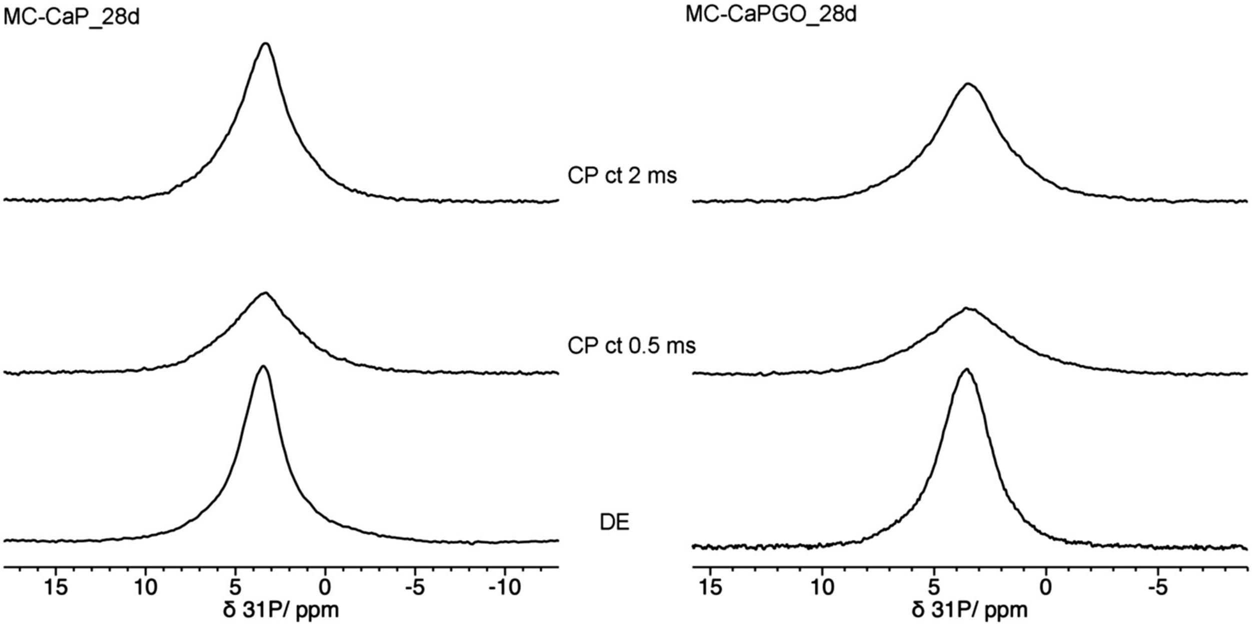

Fig. 8 $^{31}P$ MAS NMR spectra of (left) MC-CaP_28d and (right) MC-CaPGO_28d, recorded with, from bottom to top, DE experiment and CP experiments with contact times (ct) of 0.5 ms and 2 ms.

In fact, in the CP spectrum with contact time of 2 ms the narrower signal of hydroxyapatite can also be recognized. It must be mentioned that the CP spectra are much less intense than the quantitative DE-MAS spectrum, indicating that only a part of ACP is hydrogen rich. On the basis of the literature[45,48] these hydrogen atoms can be ascribed to structural water molecules present in ACP.

In order to investigate the effect of GO on the hydrogels' mineralization, $^{31}P$ and $^{1}H$ SSNMR experiments were carried out on MC-CaPGO_*x*d samples with $x = 0$, 14, and 28. The $^{31}P$ DE-MAS spectrum of the non-mineralized sample, MC-CaPGO_0d, (Fig. 6) shows that monetite is the major phase and crystalline hydroxyapatite is not present, similarly to what observed for CaPGO (Fig. S4, ESI†). On the other hand, the broad peak ascribable to ACP is observed. After 14 days in SBF, the monetite signal disappears and the narrower peak of hydroxyapatite appears, in agreement with the XRD results. After 28 days of mineralization the ACP/hydroxyapatite ratio, in terms of P atoms, is 79/21, slightly higher than in MC-CaP_28d, indicating a certain antagonistic effect of GO toward the growth of hydroxyapatite, already evident from the comparison between the $^{31}P$ spectra of CaP and CaPGO (Fig. S4, ESI†). Analogously to what observed for MC-CaP_28d, the $^{1}H$–$^{31}P$ CP-MAS spectrum of MC-CaPGO_28d with a contact time of 0.5 ms highlights the signal of ACP (Fig. 8). The $^{1}H$ MAS spectra of MC-CaP_GO_*x*d samples (Fig. 7) are very similar to those of the corresponding MC-CaP_*x*d samples, showing an intensity increase of the broad signal at 4.3 ppm with the progress of mineralization, ascribable to an increase of ACP.

### 3.3. *In vitro* biological properties

The impact of bioactivated gels, *i.e.*, gels incorporating CaP and CaPGO nanoparticles, was evaluated *in vitro* by investigating cell adhesion, proliferation and osteogenic differentiation. Previous literature has firmly established that CaP nanoparticles, synthesized *via* the sol–gel approach, exhibit notable bioactivity and osteogenic potential even under basal culture conditions.[51] Moreover, Raucci *et al.*[23] reported that biomineralized GO, synthesized using the sol–gel method at room temperature, demonstrates significant effects on cellular behavior, particularly in terms of early and late-stage osteogenic activities.

The chemical composition of the GO surface enables robust interactions with calcium phosphates, as evidenced by its active functionalities for cellular processes.[52] These unique properties of GO, combined with the bioactivity of CaP nanoparticles, suggest a synergistic effect in promoting cell adhesion and proliferation while facilitating osteogenic differentiation. These findings not only underscore the potential of CaP and CaPGO nanoparticles in tissue engineering, but also highlight the importance of understanding their interaction for optimizing biomaterial design in bone tissue regeneration applications.

In this study, we performed experiments using murine osteoblast cells (7F2) and human mesenchymal stem cells (hMSCs) to assess the effects of the developed formulations (MC, MC-CaP, MC-CaPGO) on two distinct states of cellular differentiation, as pre-differentiated in the case of 7F2 cells and undifferentiated in the case of hMSCs. By examining these specific cell types at different stages of differentiation, we aimed at gaining a comprehensive understanding of how the bioactivated MC-based hydrogels influence cellular behaviors.

First, the bioactivated formulations (MC-CaP, MC-CaPGO) were evaluated in terms of cell viability normalized to the MC hydrogel control. Considering 7F2 cells, a decline in cell viability for MC-CaP and MC-CaPGO compared to the MC control was observed at day 7 (Fig. 9A), paralleling the

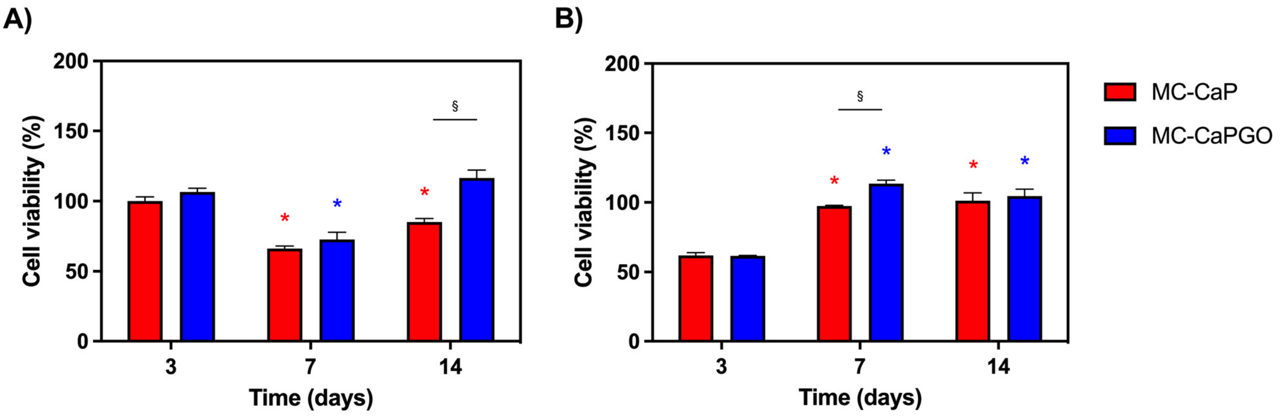

Fig. 9 Cell viability normalized with respect to MC for (A) 7F2 cells and (B) hMSCs within hydrogel formulations at 3, 7, and 14 days. $^{*}p < 0.05$ between the same formulation type (*vs.* time point 3 days); $^{\S}p < 0.05$ between different formulations (MC-CaP and MC-CaPGO) at the same time point.

transition of cells into a differentiation state (as revealed below, Fig. 10A). This transition causes a decrease in cell proliferation and subsequently reduces their metabolic activity.[53] Considering hMSCs encapsulated in MC-CaP and MC-CaPGO, an early decrease in cell viability compared to MC control occurred at day 3 (Fig. 9B). This response in undifferentiated cells may be attributed to the time required for cells to adapt to the bioactive environment. Remarkably, for both cell types, the incorporation of bioactive materials had no long-term adverse effect on cell proliferation.

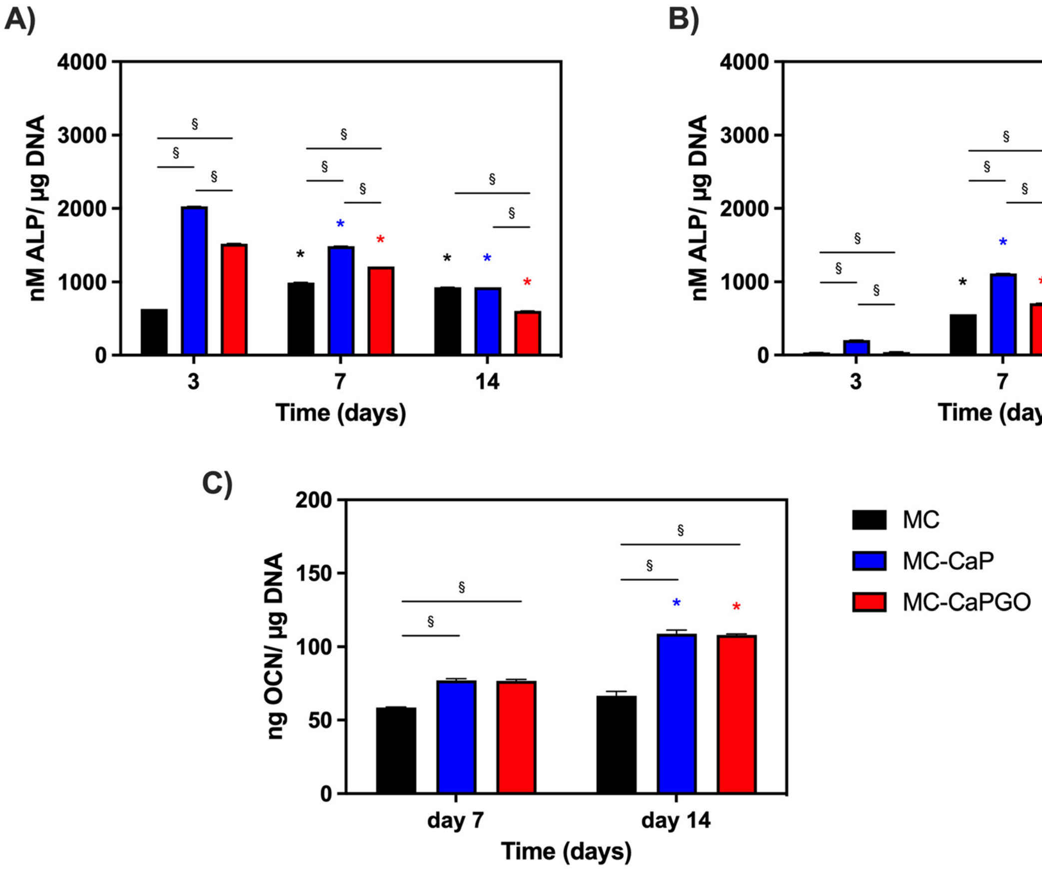

Fig. 10 *In vitro* osteogenic differentiation: (A) ALP expression of 7F2 cells after 3, 7, and 14 days of cell culture for MC-based hydrogels. $^{*}p < 0.05$ between the same formulation type (*vs.* time point 3 days); $^{\S}p < 0.05$ between different formulations (MC, MC-CaP, and MC-CaPGO) at the same time point. (B) ALP expression of hMSCs after 3, 7 and 14 days of cell culture for MC-based hydrogels, $^{*}p < 0.05$ between the same formulation type (*vs.* time point 3 days); $^{\S}p < 0.05$ between different formulations (MC, MC-CaP, and MC-CaPGO) at the same time point. (C) OCN levels of hMSCs at 7 and 14 days for MC, MC-CaP, and MC-CaGO. $^{*}p < 0.05$ between the same formulation type (7 *vs.* 14 days); $^{\S}p < 0.05$ between different formulations (MC, MC-CaP, and MC-CaPGO) at the same time point.

The effect of GO in the bioactive formulations was then investigated. By comparing MC-CaP and MC-CaPGO formulations for 7F2 cells, no significant differences in cell viability were observed at day 3 (Fig. 9A). Increased viability was observed for the MC-CaPGO formulation (*vs.* MC-CaP) at day 7. Interestingly, this difference was even more noticeable at day 14 (Fig. 9A). By comparing MC-CaP and MC-CaPGO formulations for hMSCs, the highest viability levels were instead observed for MC-CaPGO at day 7 (Fig. 9B). These results underscore the beneficial impact of incorporating GO in the hydrogel formulation, indicating its potential to enhance cell proliferation. Overall, the improved cellular response observed with MC-CaPGO suggests a conductive environment for cell adhesion and proliferation.

Furthermore, the impact of bioactivated hydrogels on osteogenic differentiation was assessed in basal medium by measuring the expression of alkaline phosphatase (ALP) and osteocalcin (OCN) as markers of early and late osteogenesis, respectively.

The results depicted in Fig. 10A and B illustrate distinct patterns of ALP expression in 7F2 cells and hMSCs over time. Notably, at day 3, the effects of the bioactivated hydrogels (MC-CaP and MC-CaPGO) were already evident for 7F2 cells. Interestingly, ALP levels decreased throughout the culture period (Fig. 10A). The response differed for hMSCs, which are undifferentiated cells with osteogenic potential at later stages. For this second cell type, higher ALP levels were observed around day 7 and by day 14 it was evident that CaPGO exhibited a more pronounced effect compared to MC-CaP (Fig. 10B).

Lastly, we focused the investigation on hMSCs to assess the impact of bioactivated formulations on osteocalcin levels (OCN) normalized to μg of DNA. This decision was based on the significance of hMSCs in bone tissue engineering and the importance of OCN as a key marker of their osteogenic differentiation. Therefore, analyzing OCN levels in hMSCs offers valuable insights into their reaction to the bioactivated formulations. The results (Fig. 10C) demonstrated that at day 7 MC-CaP and MC-CaPGO show a slight increase of OCN level compared to MC control. However, the highest levels of OCN expression were recorded at day 14. This aligns with previous studies suggesting that CaP nanoparticles and GO incorporation into hydrogels enhance osteogenic differentiation markers.[54,55]

Overall, these findings underscore the potential of bioactivated MC-based hydrogels in promoting osteogenic differentiation, as evidenced by the enhanced expression of ALP and OCN. The different responses observed between 7F2 cells and hMSCs, attributed to their different states of differentiation, highlight the importance of considering cell type-specific responses in the development of biomaterials for tissue engineering applications.

## 4. Conclusions

The thorough characterization presented in this work demonstrates that the proposed biocomposites based on MC, CaP, and CaPGO lend themselves well as potential thermo-responsive IBSs, thanks to their fast gelation (~90 s) at body temperature (37 °C), ease of injectability, and retention at the bone defect site. Thanks to these properties, the developed formulations are superior to conventional hydrogels and scaffolds, since they can be implanted *via* minimally invasive procedures, filling irregularly shaped cavities often occurring after trauma or surgery, and guaranteeing continuity into the host tissues. The addition of CaP and CaPGO led to a significant mineralization as revealed by the formation of a biomimetic phase, which was found to be constituted by crystalline hydroxyapatite and amorphous ACP through a detailed SSNMR characterization. The *in vitro* biological characterization revealed the favorable impact of CaP and CaPGO incorporation in promoting cell proliferation and osteogenic differentiation. Remarkably, the addition of GO, which is very attractive for its bioactive potential, did not negatively affect the injectability of the hydrogel nor the mineralization process, but had a positive impact in providing a conducive environment for cell growth and osteogenic differentiation on both pre-differentiated and undifferentiated cells.

Overall, the proposed formulations have the potential to be directly employed for the ultimate purpose without any modifications. In conclusion, further *in vitro* and *in vivo* assessments could open the floodgates to the development of novel, injectable formulations with potential as IBSs in bone regeneration both under physiological and pathological conditions.

## Author contributions

Conceptualization, methodology, formal analysis, investigation, writing – original draft, writing – review and editing, and visualization, L. B.; conceptualization, resources, methodology, investigation, writing – original draft, and writing – review and editing, S. B. and L. C.; methodology, investigation, writing – review and editing, A. S.; methodology and investigation, A. B.; methodology, writing – review and editing, M. G. R.; conceptualization, resources, writing – original draft, writing – review and editing, supervision, L. A.; all authors have read and agreed to the published version of the manuscript.

## Conflicts of interest

There are no conflicts to declare.

## Acknowledgements

This research was funded by Ministero dell'Università e della Ricerca (MUR), grant number PRIN 'ACTION' 2017SZ5WZB_002.

## Notes and references

1 L. Bonetti, L. De Nardo and S. Farè, *Tissue Eng., Part B*, 2021, **27**, 486–513.
2 M. L. Coughlin, L. Liberman, S. P. Ertem, J. Edmund, F. S. Bates and T. P. Lodge, *Prog. Polym. Sci.*, 2021, **112**, 101324.
3 S. Morozova, *Polym. Int.*, 2020, **69**, 125–130.

4 P. W. Schmidt, S. Morozova, S. P. Ertem, M. L. Coughlin, I. Davidovich, Y. Talmon, T. M. Reineke, F. S. Bates and T. P. Lodge, *Macromolecules*, 2020, **53**, 398–405.

5 J. R. Lott, J. W. McAllister, M. Wasbrough, R. L. Sammler, F. S. Bates and T. P. Lodge, *Macromolecules*, 2013, **46**, 9760–9771.

6 J. R. Lott, J. W. McAllister, S. A. Arvidson, F. S. Bates and T. P. Lodge, *Biomacromolecules*, 2013, **14**, 2484–2488.

7 L. Bonetti, L. De Nardo and S. Farè, *Soft Matter*, 2023, **19**, 7869–7884.

8 P. Kondiah, Y. Choonara, P. Kondiah, T. Marimuthu, P. Kumar, L. Du Toit and V. Pillay, *Molecules*, 2016, **21**, 1580.

9 A. Mellati and J. Akhtari, *Res. Mol. Med.*, 2018, **6**(4), 1–14.

10 G. A. N. Atia, H. K. Shalaby, N. G. Ali, S. M. Morsy, M. M. Ghobashy, H. A. N. Attia, P. Barai, N. Nady, A. S. Kodous and H. R. Barai, *Pharmaceuticals*, 2023, **16**, 702.

11 M. H. Kim, B. S. Kim, H. Park, J. Lee and W. H. Park, *Int. J. Biol. Macromol.*, 2018, **109**, 57–64.

12 A. Fiorati, C. Linciano, C. Galante, M. G. Raucci and L. Altomare, *Materials*, 2021, **14**, 4511.

13 Ö. Demir Oğuz and D. Ege, *Materials*, 2018, **11**, 604.

14 M. Maleki, R. Zarezadeh, M. Nouri, A. R. Sadigh, F. Pouremamali, Z. Asemi, H. S. Kafil, F. Alemi and B. Yousefi, *Biomol. Concepts*, 2020, **11**, 182–200.

15 M. H. Kim, H. Park and W. H. Park, *Carbohydr. Polym.*, 2018, **191**, 176–182.

16 H. Park, M. H. Kim, Y. I. Yoon and W. H. Park, *Carbohydr. Polym.*, 2017, **157**, 775–783.

17 L. Bonetti, L. De Nardo and S. Farè, *Gels*, 2021, **7**, 141.

18 L. Bonetti, L. D. Nardo, F. Variola and S. Farè, *Soft Matter*, 2020, **16**, 5577–5587.

19 L. Bonetti, L. De Nardo, F. Variola and S. Farè, *Mater. Lett.*, 2020, **274**, 128011.

20 L. Altomare, A. Cochis, A. Carletta, L. Rimondini and S. Farè, *J. Mater. Sci.: Mater. Med.*, 2016, **27**, 95.

21 A. Cochis, L. Bonetti, R. Sorrentino, N. Contessi Negrini, F. Grassi, M. Leigheb, L. Rimondini and S. Farè, *Materials*, 2018, **11**, 579.

22 L. Bonetti, A. Fiorati, A. D'Agostino, C. M. Pelacani, R. Chiesa, S. Farè and L. De Nardo, *Gels*, 2022, **8**, 298.

23 M. G. Raucci, D. Giugliano, A. Longo, S. Zeppetelli, G. Carotenuto and L. Ambrosio, *J. Tissue Eng. Regener. Med.*, 2017, **11**, 2204–2216.

24 J. Desbrières, M. Hirrien and S. B. Ross-Murphy, *Polymer*, 2000, **41**, 2451–2461.

25 T. Kokubo and H. Takadama, *Biomaterials*, 2006, **27**, 2907–2915.

26 R. K. Harris, E. D. Becker, S. M. Cabral De Menezes, P. Granger, R. E. Hoffman and K. W. Zilm, *Solid State Nucl. Magn. Reson.*, 2008, **33**, 41–56.

27 G. T. Gold, D. M. Varma, D. Harbottle, M. S. Gupta, S. S. Stalling, P. J. Taub and S. B. Nicoll, *J. Biomed. Mater. Res., Part A*, 2014, **102**, 4536–4544.

28 Ö. D. Oğuz and D. Ege, *MRS Commun.*, 2019, **9**, 1174–1180.

29 D. J. Overstreet, D. Dutta, S. E. Stabenfeldt and B. L. Vernon, *J. Polym. Sci., Part B: Polym. Phys.*, 2012, **50**, 881–903.

30 S. Yasmeen, M. K. Lo, S. Bajracharya and M. Roldo, *Langmuir*, 2014, **30**, 12977–12985.

31 V. Burckbuchler, G. Mekhloufi, A. P. Giteau, J. L. Grossiord, S. Huille and F. Agnely, *Eur. J. Pharm. Biopharm.*, 2010, **76**, 351–356.

32 C. Chung and J. A. Burdick, *Adv. Drug Delivery Rev.*, 2008, **60**, 243–262.

33 E. B. Hunziker, *Osteoarthritis Cartilage*, 2002, **10**, 432–463.

34 S. Ghanaati, M. Barbeck, U. Hilbig, C. Hoffmann, R. E. Unger, R. A. Sader, F. Peters and C. J. Kirkpatrick, *Acta Biomater.*, 2011, **7**, 4018–4028.

35 C. C. Lopes, W. A. Pinheiro, D. Navarro Da Rocha, J. G. Neves, A. B. Correr, J. R. M. Ferreira, R. M. Barbosa, J. R. F. Soares, J. L. Santos and M. H. Prado Da Silva, *Ceram. Int.*, 2021, **47**, 7653–7665.

36 A. Kaflak-Hachulska, A. Samoson and W. Kolodziejski, *Calcif. Tissue Int.*, 2003, **73**, 476–486.

37 M. Edén, *Materialia*, 2021, **17**, 101107.

38 Y.-Y. Hu, X. P. Liu, X. Ma, A. Rawal, T. Prozorov, M. Akinc, S. K. Mallapragada and K. Schmidt-Rohr, *Chem. Mater.*, 2011, **23**, 2481–2490.

39 R. Gelli, M. Tonelli, F. Martini, L. Calucci, S. Borsacchi and F. Ridi, *Constr. Build. Mater.*, 2022, **348**, 128686.

40 Y. Coppel, Y. Prigent and G. Grégoire, *Acta Biomater.*, 2021, **120**, 156–166.

41 Y. Yu, H. Guo, M. Pujari-Palmer, B. Stevensson, J. Grins, H. Engqvist and M. Edén, *Ceram. Int.*, 2019, **45**, 20642–20655.

42 E. E. Wilson, A. Awonusi, M. D. Morris, D. H. Kohn, M. M. J. Tecklenburg and L. W. Beck, *Biophys. J.*, 2006, **90**, 3722–3731.

43 S. Hayakawa, K. Tsuru, C. Ohtsuki and A. Osaka, *J. Am. Ceram. Soc.*, 2004, **82**, 2155–2160.

44 C. Gervais, C. Bonhomme and D. Laurencin, *Solid State Nucl. Magn. Reson.*, 2020, **107**, 101663.

45 Y. Yu, B. Stevensson, M. Pujari-Palmer, H. Guo, H. Engqvist and M. Edén, *Int. J. Mol. Sci.*, 2019, **20**, 6356.

46 W. P. Rothwell, J. S. Waugh and J. P. Yesinowski, *J. Am. Chem. Soc.*, 1980, **102**, 2637–2643.

47 S. Hayakawa, K. Tsuru, H. Iida, C. Ohtsuki and A. Osaka, *J. Ceram. Soc. Jpn.*, 1996, **104**, 1000–1003.

48 R. Mathew, P. N. Gunawidjaja, I. Izquierdo-Barba, K. Jansson, A. García, D. Arcos, M. Vallet-Regí and M. Edén, *J. Phys. Chem. C*, 2011, **115**, 20572–20582.

49 P. N. Gunawidjaja, A. Y. H. Lo, I. Izquierdo-Barba, A. García, D. Arcos, B. Stevensson, J. Grins, M. Vallet-Regí and M. Edén, *J. Phys. Chem. C*, 2010, **114**, 19345–19356.

50 E. Leonova, I. Izquierdo-Barba, D. Arcos, A. López-Noriega, N. Hedin, M. Vallet-Regí and M. Edén, *J. Phys. Chem. C*, 2008, **112**, 5552–5562.

51 B. Yuan, M. G. Raucci, Y. Fan, X. Zhu, X. Yang, X. Zhang, M. Santin and L. Ambrosio, *J. Mater. Chem. B*, 2018, **6**, 7974–7984.

52 A. Raslan, L. Saenz Del Burgo, J. Ciriza and J. L. Pedraz, *Int. J. Pharm.*, 2020, **580**, 119226.

53 M. E. Frohbergh, A. Katsman, G. P. Botta, P. Lazarovici, C. L. Schauer, U. G. K. Wegst and P. I. Lelkes, *Biomaterials*, 2012, **33**, 9167–9178.

54 J. Su, Z. Du, L. Xiao, F. Wei, Y. Yang, M. Li, Y. Qiu, J. Liu, J. Chen and Y. Xiao, *Mater. Sci. Eng., C*, 2020, **113**, 110983.

55 A. Şelaru, H. Herman, G. M. Vlăsceanu, S. Dinescu, S. Gharbia, C. Baltă, M. Roşu, C. V. Mihali, M. Ioniţă, A. Serafim, H. Iovu, A. Hermenean and M. Costache, *IJMS*, 2022, **23**, 491.